N90-12535

THEORETICAL METHODS AND DESIGN STUDIES FOR NLF AND HLFC SWEPT WINGS AT SUBSONIC AND SUPERSONIC SPEEDS

Suresh H. Goradia
Vigyan Research Associates
Hampton, Virginia

Harry L. Morgan, Jr.
NASA Langley Research Center
Hampton, Virginia

INTRODUCTION

Laminarization of the boundary layer on the surface of aircraft wings can be accomplished by the use of concepts such as Natural Laminar Flow (NLF), Laminar-Flow Control (LFC) which uses suction over the entire surface of the wing, and Hybrid Laminar-Flow Control (HLFC) which uses suction only over 15 to 20 percent of the wing upper surface near the leading edge. The experimental data obtained at NASA Langley for the LFC wing have demonstrated that substantial reductions in wing profile drag can be obtained at transonic Mach numbers by the use of suction over the entire surface of the airfoil.[1] This drag reduction is primarily the result of the presence of laminar boundary-layer flow over a large portion of the airfoil surface.

Extension regions of laminar flow can also be maintained on wing surfaces with the NLF concept, which involves the appropriate choice of pressure distribution to limit the amplification of the disturbances that trigger the transition of the laminar boundary layer to a turbulent boundary layer. Flight tests at the Dryden Flight Research Center on a variable sweep TACT F-111 fighter aircraft with an NLF wing glove have shown that laminar flow can be maintained over a large portion of the wing surface at transonic speeds.[2] However, NLF is restricted to flight applications at low Reynolds number conditions and to wings with relatively low sweep angles.

HLFC which combines the features of both LFC and NLF applies suction forward of the front wing-box spar to prevent the transition of the laminar boundary layer due to cross-flow and attachment-line instabilities that occur on swept wings. Laminar boundary-layer flow is maintained aft of the front spar by the selection of a pressure distribution which surpresses the growth of the disturbances due to Tollmien-Schlichting waves or due to cross flow. Although the extent of laminar flow is less for HLFC than for LFC, the conventional wing box structure can be retained and the mechanical complexities are not as great.

The design of the HLFC wing sections to minimize the wake drag requires the optimization of the drag due to laminar skin-friction and the turbulent boundary-layer separation. The trailing-edge recovery pressure is fixed due to the Kutta condition for subsonic and transonic flow and the aft pressure gradient, free-stream Reynolds number, and forward suction levels determine whether or not the turbulent flow will remain attached close to the trailing edge. Examination of existing experimental data on the LFC wing has shown that if turbulent separation occurs upstream of the 95-percent chord position on either the upper or lower wing surfaces, a pressure distribution necessary to maintain laminar flow cannot be realized. Therefore, the design of HLFC wings sections necessitates the use of reliable theoretical methods which accurately predict the locations of laminar boundary-layer transition and turbulent boundary-layer separation.

Several finite-difference boundary layer, stability, and full Navier-Stokes equation solvers are available and have produced very encouraging results. However, these methods are not well suited for the routine optimization studies that were performed during the design of the HLFC wing section. Several new integral boundary-layer methods, which are applicable to swept wings with varying amounts of surface suction, have been developed for the prediction of laminar, transition, and separating turbulent boundary layers. These methods have been developed for use at either subsonic or supersonic speeds, have small computer execution times, and are simple to use. The purpose of this presentation is to briefly outline the theoretical equations and assumptions which form the basis of these boundary-layer

methods and to present the results of several correlation cases with existing experimental data. The results of the application of these methods to the design of the HLFC wing scheduled to be tested in the Langley 8-Foot Transonic Pressure Tunnel will also be presented.

THEORETICAL METHODS USED DURING DESIGN OF HLFC WING

The theoretical methods used during the design and analysis of the HLFC wing are listed in figure 1 and are classified as 1) potential/viscous design and analysis, 2) boundary-layer analysis, 3) wake and suction drag computations, and 4) a modified strip method for finite wings.

Design of the upper surface of the HLFC wing in the local supersonic region at the design transonic free-stream Mach number was performed using the Perturbation Method of Characteristics technique.[3] Modifications to the HLFC airfoil section were analyzed at transonic conditions using the Korn/Garabedian airfoil code[4] and at subsonic conditions using the Multi-Component (MCARF) airfoil code.[5]

Analysis of design modifications on the viscous characteristics of the HLFC wing were performed using several recently developed integral boundary-layer methods. These methods consist of 1) an integral compressible laminar boundary-layer method for swept wings in the presence of suction at subsonic and supersonic speeds, 2) criteria for prediction of laminar boundary-layer separation and reattachment,[6] 3) criteria for prediction of the location transition due to either the amplification of Tollmien-Schlichting waves, cross flow, or leading-edge contamination,[7] and 4) new integral separating turbulent boundary layer.

Theoretical methods were also developed to determine the effect of design modifications on the drag characteristics of the HLFC wing. These methods account for both the changes in the wake drag and suction drag as a result of applying suction on the upper surface leading-edge region of the HLFC airfoil.

A modified strip method was developed during this design study to account for the finite and swept wing properties of the HLFC wing. This strip method also accounts for taper and both spanwise and chordwise pressure gradients.

- Potential/viscous design and analysis
  - Perturbation method of characteristics for inverse design at transonic speeds
  - BGK (Bauer-Garabedian-Korn) for transonic analysis
  - MCARF for subsonic analysis
- Boundary-layer analysis
  - Integral compressible laminar boundary layer with sweep and suction at subsonic thru supersonic speeds
  - Short bubble and reattachment criteria
  - T.S. and C.F. transition criteria
  - Separating turbulent boundary layer method (AIAA 86-1832-CP)
- $C_{D,\,wake}$ and $C_{D,\,suction}$
- Modified strip method

Figure 1

GOVERNING EQUATIONS

The usual governing equations for compressible hydrodynamic laminar boundary-layer flow which consist of the continuity, streamwise-momentum, normal-momentum, and cross-flow-momentum equations are presented in figure 2. These equations contain the terms consisting of variable physical properties, such as, density, ρ, and dynamic viscosity, μ. The values of these physical properties vary across the boundary layer as well as along the flow direction, and these variations are non-negligible for boundary-layer flow at transonic speeds. At supersonic speeds, these variations in the physical properties of fluid within the boundary layer are quite appreciable. This means that there is a strong coupling between solutions of hydrodynamic and thermal boundary-layer equations at high transonic and supersonic speeds.

In order to simplify the governing equations for solution by integral techniques while maintaining realistic, computational results for the hydrodynamic and thermal boundary layers, Stewartson's transformations are used. These transformations reformulate the boundary-layer equations of motions into a transformed plane which is independent of the varying physical properties of fluid. The relations between the velocities in the transformed and physical planes are also shown in figure 2.

GOVERNING EQUATIONS AND TRANSFORMATIONS

GOVERNING EQUATIONS

$$\frac{\partial}{\partial s}(\rho u) + \frac{\partial}{\partial \xi}(\rho v) + \frac{\partial}{\partial z}(\rho w) = 0 \quad \text{(Continuity)}$$

$$\rho u \frac{\partial u}{\partial s} + \rho v \frac{\partial u}{\partial \xi} + \rho w \frac{\partial u}{\partial z} = -\frac{dP}{ds} + \frac{\partial}{\partial \xi}\left(\mu \frac{\partial u}{\partial \xi}\right) \quad \text{(Streamwise Momentum)}$$

$$\frac{\partial P}{\partial \xi} = 0 \quad \text{(Normal Momentum)}$$

$$\rho u \frac{\partial w}{\partial s} + \rho v \frac{\partial w}{\partial \xi} + \rho w \frac{\partial w}{\partial z} = -\frac{\partial P}{\partial z} + \frac{\partial}{\partial \xi}\left(\mu \frac{\partial w}{\partial z}\right) \quad \text{(Crossflow Momentum)}$$

Stewartson's Transformation

$$X = \int_0^s \frac{a_e P_e}{a_o P_o}\, ds; \quad Y = \frac{a_e}{a_o} \int_0^\xi \frac{\rho}{\rho_o}\, d\xi$$

Relation Between Velocities in Physical and Transformed Planes

$$U = \frac{a_o}{a_e} u; \quad V = \frac{a_o}{a_e} v \text{ for } P_r = 1; \quad W = w$$

Figure 2

TRANSFORMED BOUNDARY-LAYER EQUATIONS AND BOUNDARY CONDITIONS

The transformed boundary-layer equations using Stewartson's tranformations are presented in figure 3. These tranformed boundary-layer equations are applicable to infinite swept wings. The relation between the pressure gradient in the transformed and physical planes and the transformed boundary conditions needed to derive the integral equations is also shown. The several groups of physical dimensionless parameters used in the development of the integral compressible boundary-layer method are also presented. The subscript "w" indicates that the parameter is defined at the wall.

TRANSFORMED BOUNDARY LAYER EQUATIONS

$$\frac{\partial U}{\partial X} + \frac{\partial V}{\partial Y} = 0$$

$$U \frac{\partial U}{\partial X} + V \frac{\partial U}{\partial Y} = U_e \frac{dU_e}{dX} + \nu_o \frac{\partial^2 U}{\partial Y^2}$$

$$U \frac{\partial W}{\partial X} + V \frac{\partial W}{\partial Y} = \nu_o \frac{\partial W}{\partial Y^2}$$

$$\frac{dU_e}{dX} = \frac{1}{\lambda} a_o \frac{dM_e}{ds} \left(1 + \frac{\gamma - 1}{2} M_e^2\right)^4$$

where $$\lambda = \left(\frac{T_w}{T_o}\right)^{1/2} \left(\frac{T_o + 198.6}{T_w + 198.6}\right) \text{ and } \frac{\mu}{\mu_o} = \lambda \frac{T}{T_o}$$

Boundary Conditions in Transformed Plane

$$@\ Y = 0 \rightarrow U = W = 0,\ V = V_s = -\frac{a_o}{a_e} v_o$$

$$@\ Y = \delta_s \rightarrow U = U_e = a_o M_e,\ \frac{\partial U}{\partial Y} = \frac{\partial^2 U}{\partial Y^2} = 0$$

$$@\ Y = \delta_z \rightarrow W = W_e = w_e,\ \frac{\partial W}{\partial Y} = \frac{\partial^2 W}{\partial Y^2} = 0$$

Define

$$L = \theta_s \left(\frac{\partial U}{\partial Y}\right)_w;\ S = \frac{V_s \theta_s}{\nu_o};\ K = \frac{\theta_s^2}{\nu_o} \frac{dU_e}{dX}$$

$$M = \frac{\theta_s^2}{U_e} \left(\frac{\partial^2 U}{\partial Y}\right)_w;\ N = \frac{\theta_{s,tra}^3}{U_e} \left(\frac{\partial^3 U}{\partial Y^3}\right)_w$$

Figure 3

COMPATIBILITY CONDITIONS AND STREAMWISE MOMENTUM-INTEGRAL EQUATION WITH SUCTION

The compatibility conditions used to derive the integral boundary-layer equations are presented in figure 4. The streamwise momentum-integral equation with suction included was derived by integrating the transformed boundary-layer equations from the wall to the edge of the boundary layer and by making use of Leibnitz's rule. Furthermore, by making use of the dimensionless parameters defined on figure 3, a set of simultaneous equations is derived for the solution for the boundary-layer momentum thickness and form factor in the transformed plane in the presence of suction. The form of function $F(S,K_s)$ is derived by the curve fit of the exact solution results for the Falkner-Skan type flow in the presence of suction.

Compatibility Conditions

$$@\ Y = 0 \rightarrow\ -V_s \left(\frac{\partial U}{\partial Y}\right)_w = U_e \frac{dU_e}{dX} + \nu_o \left(\frac{\partial^2 U}{\partial Y^2}\right)_w$$

$$@\ Y = 0 \rightarrow\ -V_s \left(\frac{\partial^2 U}{\partial Y^2}\right)_w = \nu_o \left(\frac{\partial^3 U}{\partial Y^3}\right)_w$$

$$@\ Y = 0 \rightarrow\ -V_s \left(\frac{\partial W}{\partial Y}\right)_w = \nu_o \left(\frac{\partial^2 W}{\partial Y^2}\right)$$

Streamwise Momentum Integral Equation in Transformed Plane

$$\frac{d\theta_s}{dX} + \frac{\theta_s}{U_e}\frac{dU_e}{dX}(H_s + 2) = \frac{\nu_o}{U_e^2}\left(\frac{\partial U}{\partial Y}\right) - \frac{V_s}{U_e}$$

Integral Equation Up To Transonic Mach Number

$$U_e \frac{d}{dX}\left\{\frac{K}{(dU_e/dX)}\right\} = 2\left[L - K_s(H_s + 2) - S\right]$$

$$= F(S, K_s)$$

where

$$F(S, K_s) = 0.44 + 5.56903K_s + 3.19594K^2 - 6.35857K^3 - 1.28S + 0.76S^2$$

and $K_s = -M - L \cdot S$

Figure 4

BOUNDARY-LAYER PARAMETERS AND CROSS FLOW MOMENTUM-INTEGRAL EQUATION

The application of reverse Stewartson's transformations yields the relationships between the parameters in the physical and transformed planes as presented in figure 5. The transformed cross-flow momentum-integral equation is derived in a manner similar to that for the streamwise momentum-integral equation. The numerical solution of this equation gives the computational results in the transformed plane in the form of the ratio of the boundary-layer thickness in the cross-flow direction to that in the streamwise direction as a function of the dimensionless parameter, S, which is the ratio of the distance along the normal section in the streamwise direction to the chord of normal section. The cross-flow boundary-layer thickness, δ_z, can be calculated by multiplying the ratio δ_z/δ_s, which is obtained by solving the cross-flow momentum-integral equation, by the streamwise boundary-layer thickness δ_s. The dimensionless shape of the velocity profile w/W_e can immediately be calculated from the knowledge of δ_z, momentum thickness, and displacement thickness.

Relation Between Physical and Transformed Boundary Layer Parameters

$$\delta_s = \theta_s \cdot F_1 (K_s, S)$$

where

$$F_1 (K_s, S) = .032 + 73.1K_s + 10.587K_s^2 - 129.6K_s^3 + 4669.6K_s^4 + 43865K_s^5$$

$$\theta_{s_{Phy}} = \theta_s \left(1 + \frac{\gamma - 1}{2} M_e\right)^3; \quad H_{s_{Phy}} = H_s \left(1 + P_r \frac{\gamma - 1}{2} M_e^2\right) + \frac{\gamma - 1}{2} M_e^2$$

$$\delta_{s_{Phy}} = \theta_{sPhy} \left[\frac{\delta_s}{\theta_s} + \frac{\gamma - 1}{2} M_e^2 (H_s + 1)\right]$$

Cross-flow Momentum Integral Equation in Transformed Plane

$$\frac{d}{dX} \left[U_e W_e \int_0^{\delta_t} \left\{\frac{U}{U_e} \left(1 - \frac{W}{W_e}\right) dY\right] = \nu_o \left(\frac{\partial W}{\partial Y}\right)_w - V_s W_e$$

where δ_t is greater of δ_s or δ_z

$$\frac{W}{W_e} = 2\eta_z - 2\eta_z^3 + \eta_z^4; \text{ where } \eta_z = \frac{Y}{\delta_z}$$

$$\frac{U}{U_e} = A_1 \eta_s + A_2 \eta_s^2 + A_3 \eta_s^3 + A_4 \eta_s^4 ; \text{ where } \eta_s = \frac{Y}{\delta_s}$$

$$A_1 = 2 + \frac{\delta_s^2}{6\nu_o} \frac{dU_e}{dX}; \quad A_2 = -0.5 \frac{\delta_s^2}{\nu_o} \frac{dU_e}{dX}; \quad A_3 = -2 - A_2; \quad A_4 = 3 - A_1$$

Figure 5

THERMAL BOUNDARY-LAYER EQUATIONS

Equations for thermal boundary layers in transformed and physical planes are presented in figure 6. As a first approximation, assuming that the external pressure gradient is negligible (which is approximately the case for the supersonic wing at low lift cruise conditions) and that the Prandtl number is close to unity, an analytical expression for the temperature profile can be derived. This expression is then modified as shown to account for real pressure gradients and the exact value of Prandtl number. The real pressure gradient is accounted for through the polynominal expression for the velocity ratio u/U_e where the A_i's are functions of the local pressure gradient. Once the temperature profiles are computed, the variations of dynamic viscosity, kinematic viscosity, and density across the boundary layer can be calculated and their average values determined. These averaged values are then utilized to compute dimensionless parameters which are used to determine the transition location of the laminar boundary layer.

Thermal Boundary Layer Equation in Physical Coordinate System

$$\rho g C_p \left(u \frac{\partial T}{\partial s} + v \frac{\partial T}{\partial \xi}\right) = u\frac{dP}{ds} - \frac{\partial}{\partial \xi}\left(K \frac{\partial T}{\partial \xi}\right) + \mu \left(\frac{\partial U}{\partial Y}\right)^2$$

$$\frac{dP}{ds} = -\rho_e U_e \frac{dU_e}{ds} = \rho_e g C_p \frac{dT_e}{ds}; \quad \rho(s, \xi)\, T(s, \xi) = \rho_e(s)\, T_e(s)$$

Equation in Transformal Coordinate System

$$U_e \frac{dU_e}{dX}\left(gC_p \frac{dT}{dU} + U\right) + \nu_o C_p \frac{P_r - 1}{P_r}\left(\frac{dT}{dU}\right)\frac{\partial^2 U}{\partial Y^2} = \alpha\left(\frac{d^2T}{dU^2} C_p + P_r\right)\left(\frac{\partial U}{\partial Y}\right)^2$$

Assume as a first approximation (i) zero pressure gradient and then (ii) $P_r = 1$

$$@\ Y = 0,\ U = 0,\ T = T_w;\ @\ Y = \infty,\ U = U_e = U_\infty,\ T = T_e = T_\infty$$

$$\frac{T - T_w}{T_e} = \frac{T_w - T_{aw}}{T_e}\left(\frac{U}{U_e}\right) - \sqrt{P_r}\ \frac{U_e^2}{2gC_pT_o}\left(\frac{U}{U_e}\right)^2$$

where,

$$\frac{U}{U_e} = A_1\eta_s + A_2\eta_s^2 + A_3\eta_s^3 + A_4\eta_s^4$$

$$T_{aw} = T_e\left(1 + \sqrt{P_r}\ \frac{\gamma - 1}{2} M_e^2\right)$$

$$\nu_m = \frac{1}{\delta_{phy}} \int_0^{\delta_{phy}} \nu d\xi; \quad \nu = \nu_o \left(1 + \frac{\gamma - 1}{2} M_e^2\right)^{1.5} \left(\frac{T}{T_e}\right)^2$$

Figure 6

CRITERIA FOR DETERMINING LOCATION OF BOUNDARY-LAYER NEUTRAL INSTABILITY

The relationship between the dimensionless pressure-gradient parameter and an "equivalent" Reynolds number based on momentum thickness for neutral instability is presented in figure 7. The curve presented is used for determining the location of neutral instability for either the streamwise or cross-flow laminar boundary layer. The effects of pressure gradients, Mach number less than 1.3, and suction were accounted for during the derivation of this curve from the solution of Orr-Sommerfeld equations in conjunction with Stewartson's transformations.

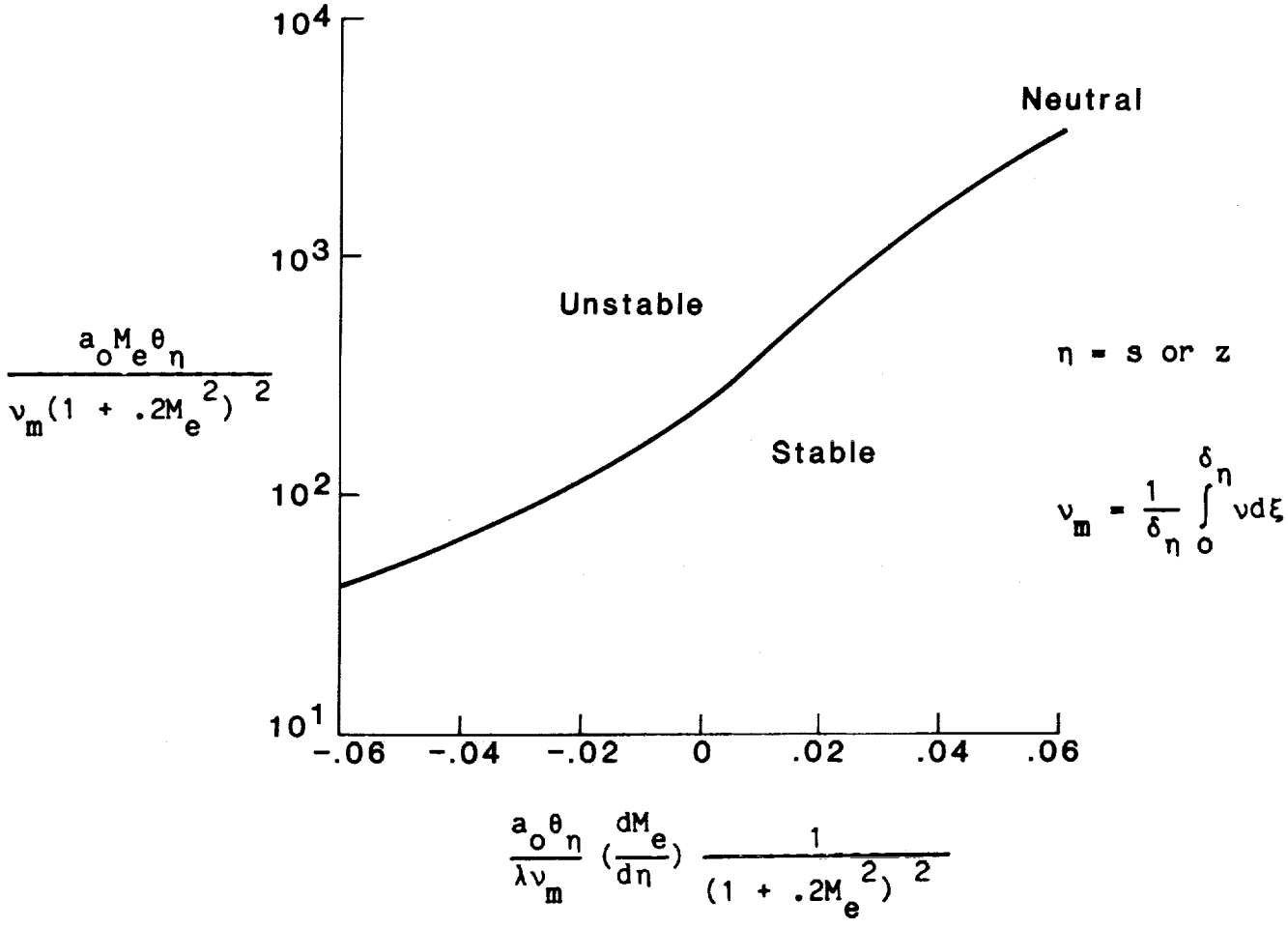

Figure 7

EFFECT OF FREE-STREAM TURBULENCE ON DIFFERENCE BETWEEN TRANSITION- AND NEUTRAL-INSTABILITY REYNOLDS NUMBER FOR FLOW ON A FLAT PLATE

The effect of free-stream turbulence on the transition location on a flat-plate laminar boundary-layer subjected to zero pressure gradient is shown in figure 8. The transition data were obtained by several investigators in the range of free-stream Mach numbers from low subsonic to a supersonic value of 3. The temperature profile data used to construct this curve were obtained either from experimental data or calculated from the previously stated theoretical expression for the temperature profile presented in figure 6. The curve shows the difference in "equivalent" Reynolds number at the transition location and at the point of neutral stability. The equations for the averaged value of kinematic viscosity ν and "equivalent" integral thickness δ^* which were used to derive this curve from the experimental data are also presented.

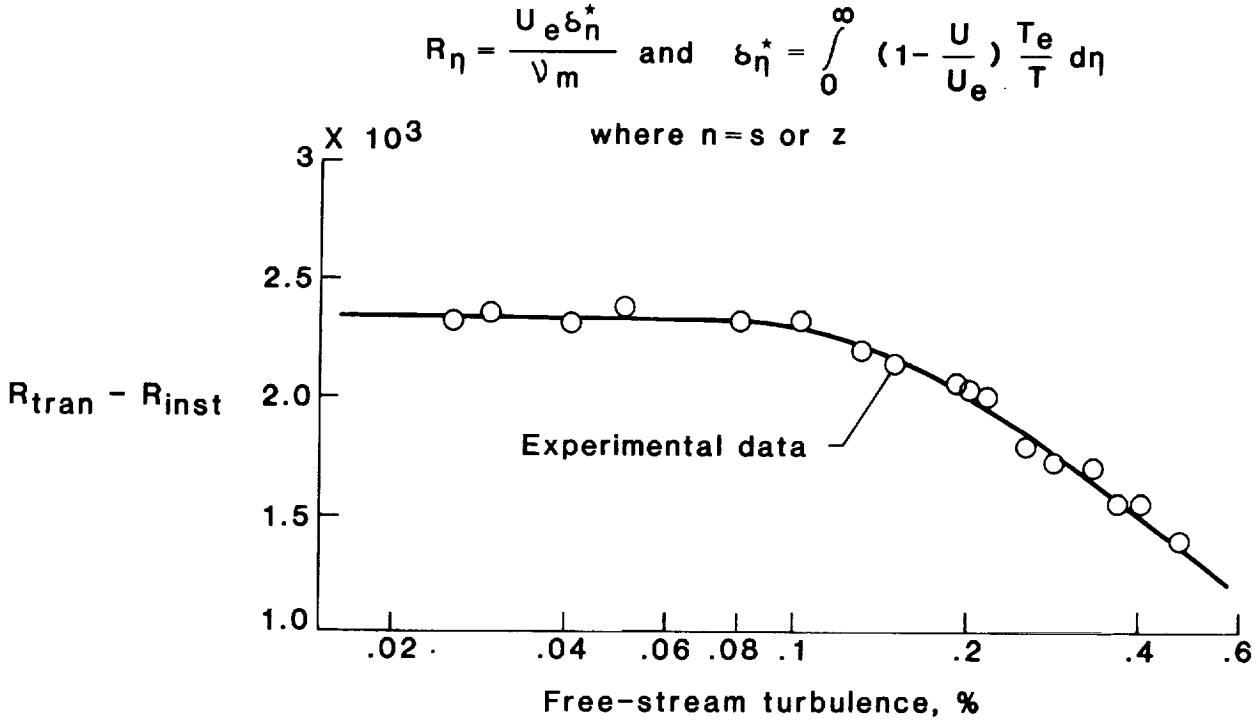

Figure 8

BOUNDARY-LAYER TRANSITION CRITERIA

The criteria used in the compressible laminar boundary-layer method to determine the transition location due either to the amplification of Tollmien-Schlichting waves or to cross flow is presented in figure 9. The dimensionless expression on the abscissa contains several implicit and explicit physical parameters that are significant during the transition of laminar boundary layer. In deriving the curves shown in this figure for several values of free-stream turbulence intensities, use has been made of information presented in figure 8. It was assumed that the effect of free-stream turbulence on the transition of laminar boundary layer without a pressure gradient behaves in a manner similar to a laminar boundary layer with a pressure gradient.

$$X = \frac{\int_{\eta_{inst}}^{\eta} \delta_\eta^* \left(\frac{T_o}{T_e}\right)^{-6} \frac{a_o}{\lambda} \frac{dM_e}{d\eta}\, d\eta}{\int_{\eta_{inst}}^{\eta} \nu_m \lambda \left(\frac{T_o}{T_e}\right)^{-4} d\eta}, \quad \text{where } \eta = s \text{ or } z$$

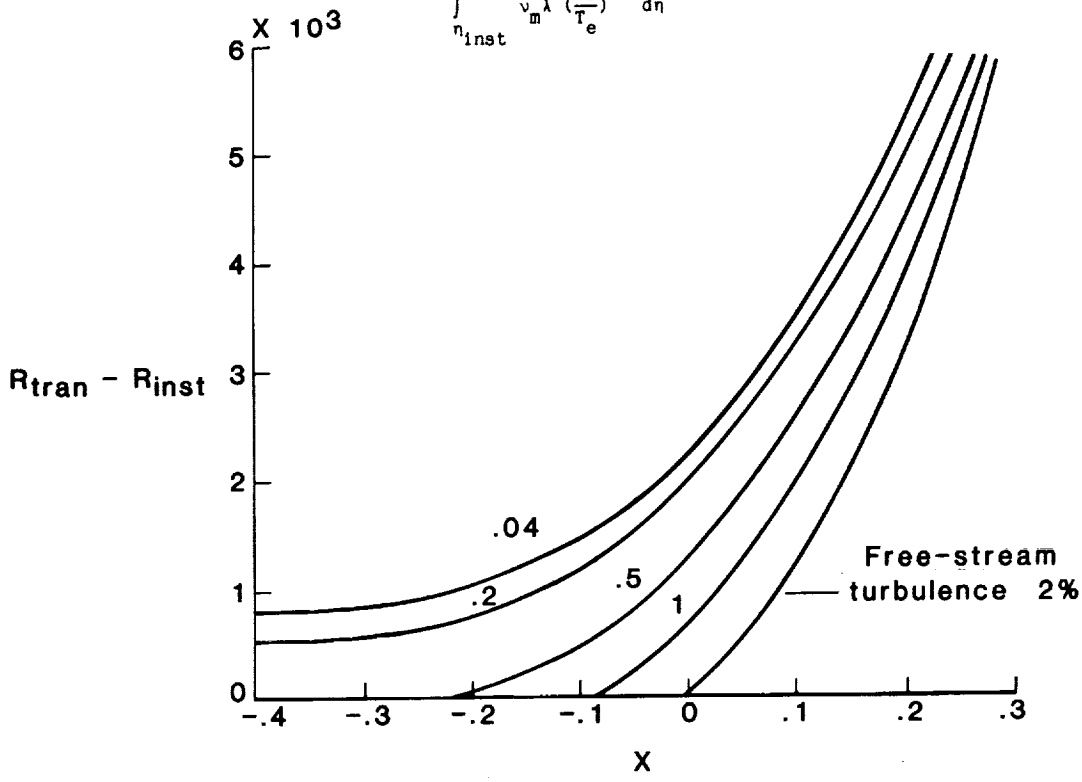

Figure 9

EQUATIONS FROM APPLICATION OF SWEEP THEORY

A schematic illustrating the application of "Strip Theory" for the prediction of laminar boundary-layer transition on a finite swept, tapered, and twisted wing is presented in figure 10. The wing is divided into a large number of finite strips oriented normal to the leading edge (more accurately normal to the local aerodynamic center-of-pressure line). The pressure distribution C_p on the edge as well as on the centerline of each strip can be determined either by the available two- or three-dimensional theoretical flow codes. The local Mach number distributions in the direction parallel and normal to the strip are also presented in this figure. These local Mach number distributions, $M_{l,s}$ and $M_{l,n}$, are input into the compressible laminar boundary-layer method to determine whether or not transition will occur due to either Tollmien-Schlichting waves or cross-flow instabilities.

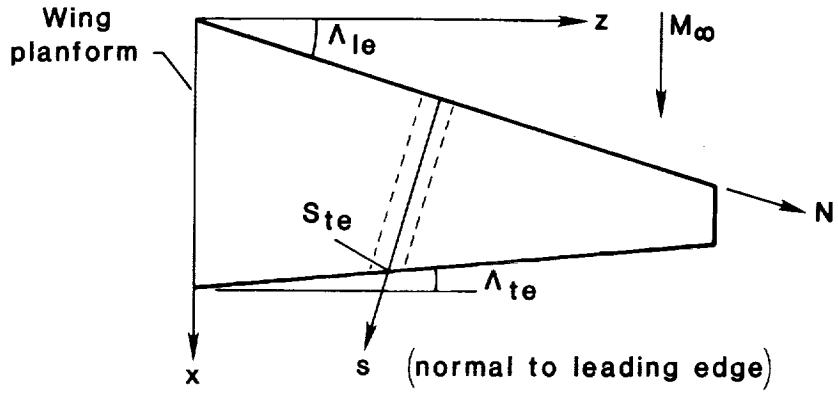

- $\Lambda_{l(local)} = \Lambda_{le} + (\Lambda_{te} - \Lambda_{le})\ (s/s_{te})$
- $(y/c)_l = (y/c)_\infty / \cos(\Lambda_l)$
- $M_S = M_\infty \cos(\Lambda_l)$, $M_N = M_\infty \sin(\Lambda_l)$
- $C_p = C_{p,s}$ (on normal section)
- $M_{l,s} = \left[5\left(1 - (1 + .2M_s^2)/(1 + .7C_pM_s^2)^{2/7}\right)\right]^{1/2}$
- $M_{l,n} = \left[5\left(1 - (1 + .2M_N^2)/(1 + .7C_pM_N^2)^{2/7}\right)\right]^{1/2}$

Figure 10

CORRELATIVE STUDIES

The present integral boundary-layer method for predicting transition was used extensively during the design of the Hybrid Laminar-Flow Control (HLFC) wing to be tested in the Langley 8-Foot Transonic Pressure Wind Tunnel. In order to establish the validity of the method prior to design of the HLFC wing, the correlative studies listed in figure 11 were performed to compare the computational results by the present theory with available experimental data.

- Variable sweep wing with NACA 64_2A015 section
- Phoenix wing
- NASA LFC wing

Figure 11

EXPERIMENTAL SETUP FOR TRANSITION MEASUREMENTS ON NASA AMES VARIABLE SWEEP WING

A schematic of the experimental setup used by Boltz[8] in the NASA Ames Research Center's 12-Foot Pressure Tunnel to determine the transition location on an infinitely swept wing at various sweep angles is shown in figure 12. The sweep angle was varied from 0° to 50° by insertion of wedges, and the wing tips were kept parallel to the free stream with appropriate wing tip extension. The wing section was an NACA 64_2A015 airfoil. The chord of the wing was four feet, and the wing was mounted vertically on the turntable in a semispan manner. In the unswept position the wing had an effective aspect ratio of 5.0. The transition locations were experimentally determined at the various sweep angles and Reynolds numbers using both flow visualization techniques and small microphones located in the model.

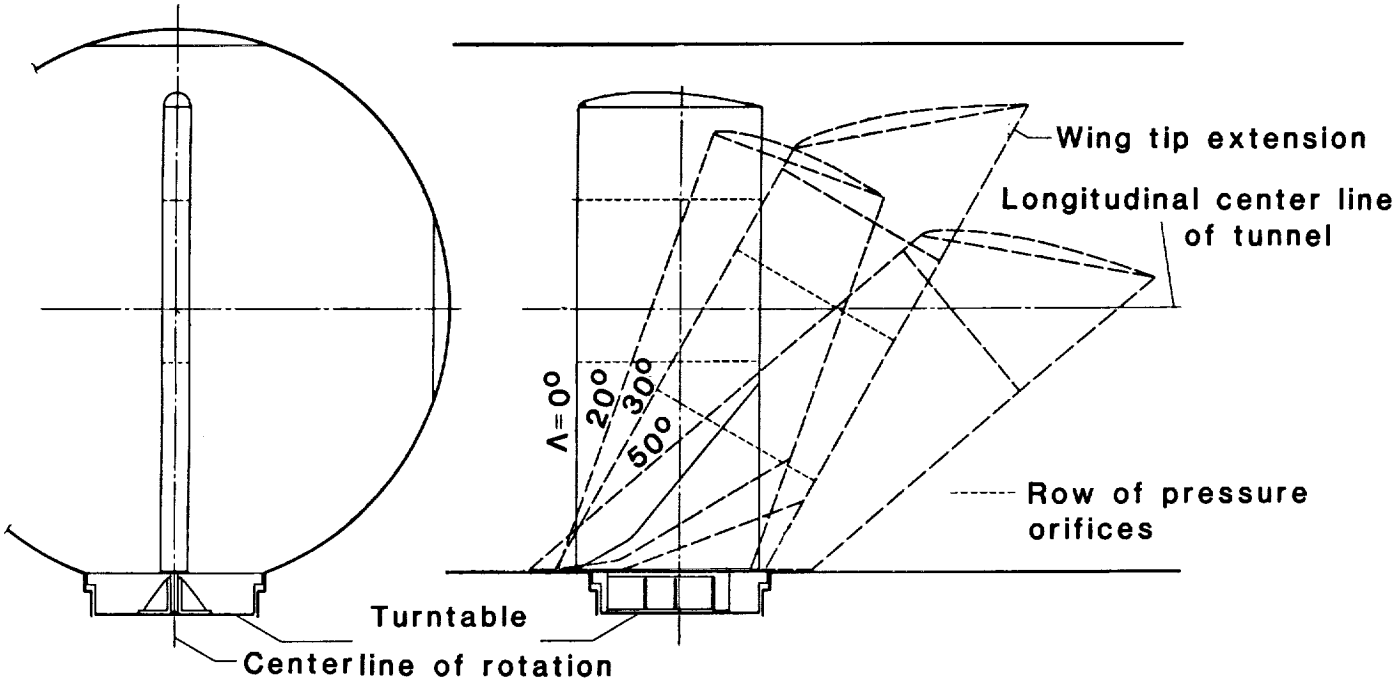

Figure 12

COMPARISON OF PRESSURE DISTRIBUTION FOR NACA 64_2A015 WING WITH 30° SWEEP

The pressure distribution computed by the NASA Multi-Component Airfoil Program (MCARF) for the NACA 64_2A015 section at an angle of attack of 1° and sweep angle of 30° is shown in figure 13. The experimental data shown in this figure were obtained by Boltz at the same free-stream conditions and sweep. The comparison shows excellent agreement between theory and experiment.

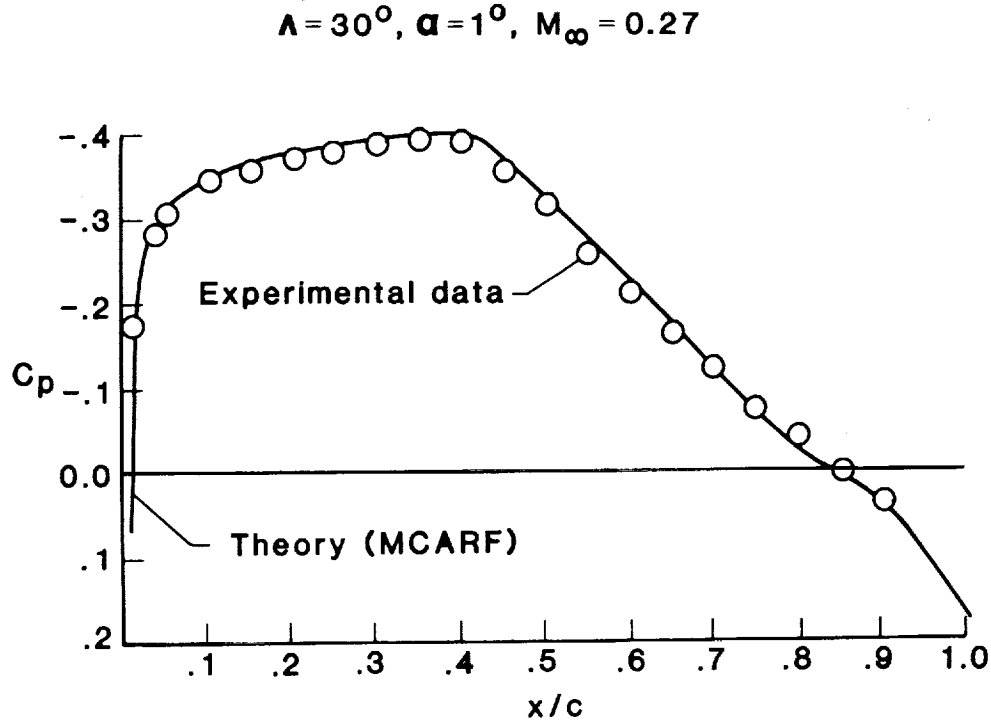

Figure 13

COMPARISON OF PRESSURE DISTRIBUTION FOR NACA 64_2A015 WING WITH 50° SWEEP

The comparison between the theoretically computed pressure distribution and experimental data by Boltz for an angle of attack of 0° and a sweep angle of 50° is shown in figure 14. The computed pressure distribution agrees quite well with the experimental data except in the vicinity of the trailing edge. This discrepancy at the trailing edge can be attributed to turbulent separation due to outboard washout phenomenon which usually occurs at this relatively high sweep angle.

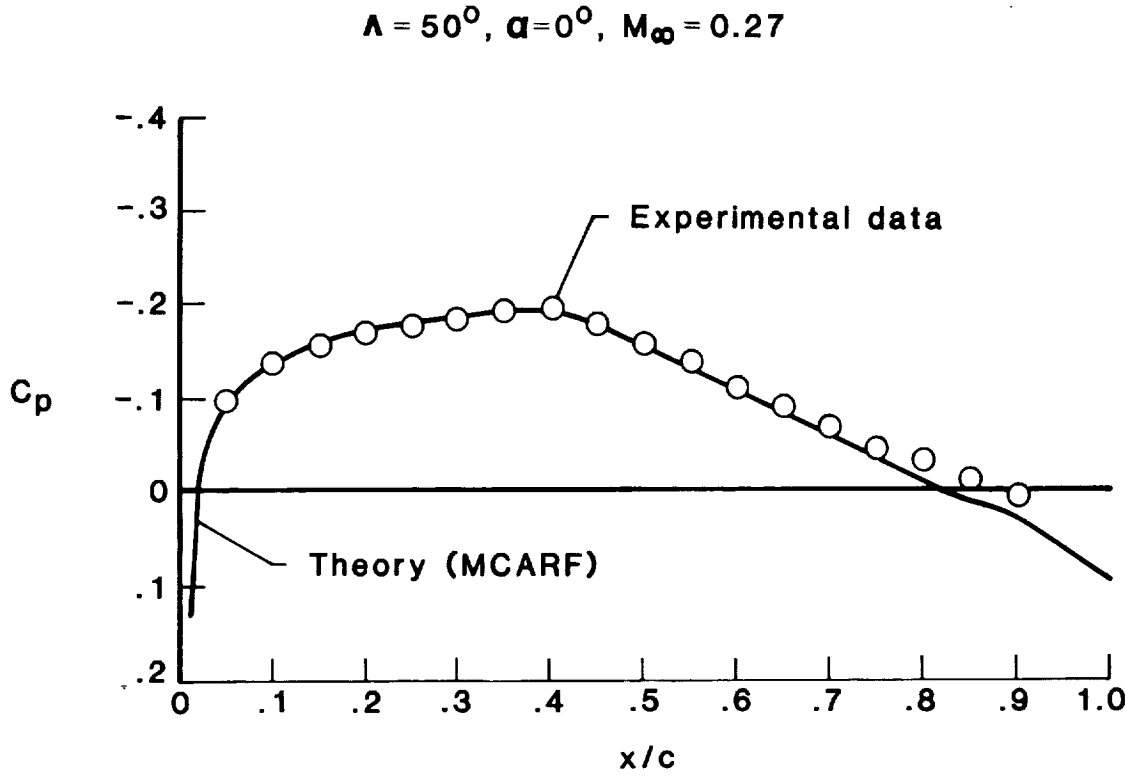

Figure 14

TRANSITION CORRELATION FOR NACA 64_2A015 WING WITH 20° SWEEP

The comparison between predicted and experimentally measured transition locations for the NACA 64_2A015 wing with 20° of sweep is presented in figure 15. The theoretical results are shown as a function of free-stream Reynolds number for transition locations due to 1) Tollmien-Schlichting waves or laminar separation with short bubble turbulent reattachment and 2) transition due to cross flow. Also shown in this figure are the computed x/c locations for Tollmien-Schlichting (T.S.) and cross-flow (C.F.) neutral instabilities as a function of free-stream Reynolds number. The correlation results suggest the following:

(1) Predicted transition due to T.S. by the present method agrees quite well with experimental data for Reynolds numbers less than 20 million.

(2) For Reynolds numbers greater than 20 million, the predicted transition due to C.F. occurs upstream of that due to T.S., and the predicted locations due to C.F. agree well with the experimental data.

(3) For a sweep of 20° and Reynolds numbers greater than 20 million, the transition is due completely to C.F.

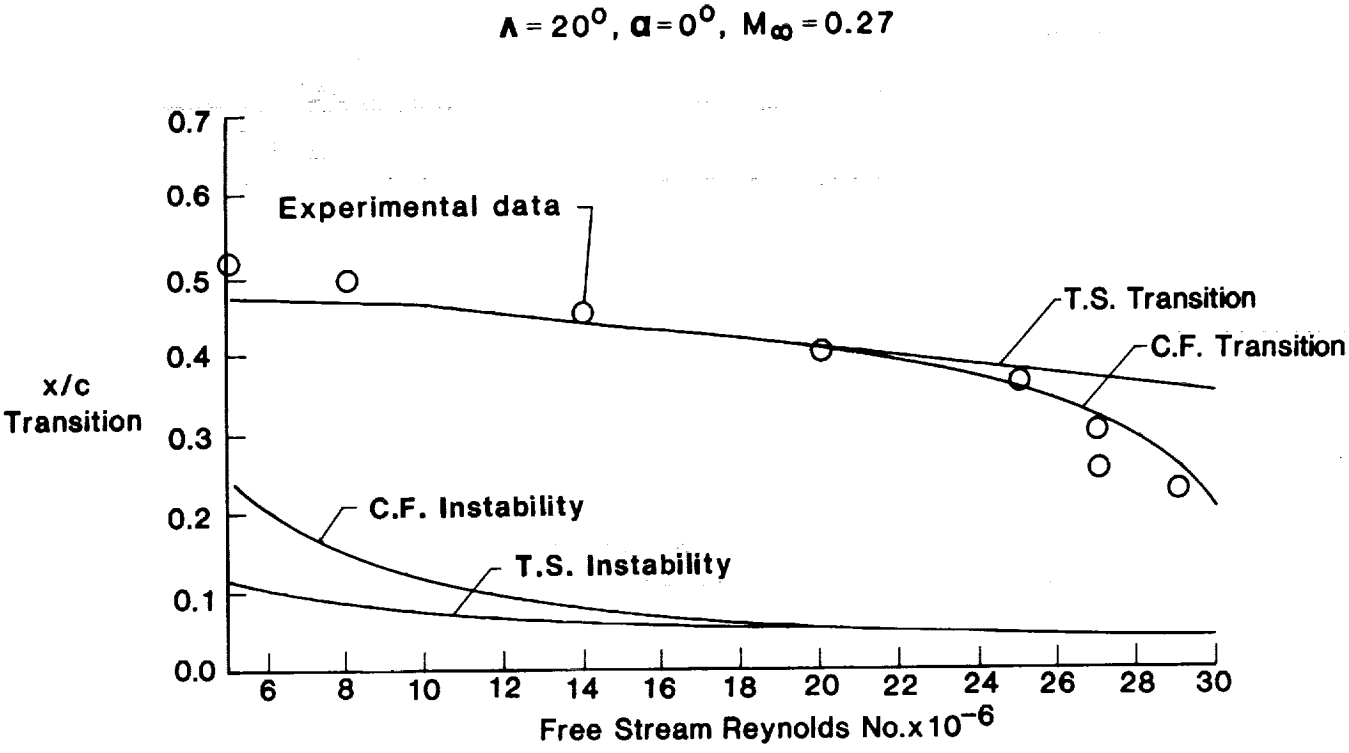

Figure 15

TRANSITION CORRELATION FOR NACA 64_2A015 WITH THE 40° SWEEP

The correlation of results between present method and Boltz's experimental data for the higher sweep angle of 40° is presented in figure 16. The theoretical data presented were computed using the pressure distribution generated by the MCARF program. The following conclusions can be drawn from the correlations presented in this figure:

(1) Transition locations due to T.S. and C.F. are predicted fairly well.

(2) For Reynolds numbers greater than 8 million, theoretical computations indicate that C.F. triggers the transition more abruptly and earlier than at the lower sweep angles.

(3) There is a danger of leading-edge contamination due to C.F. for Reynolds numbers larger than 18 million at a sweep angle of 40°.

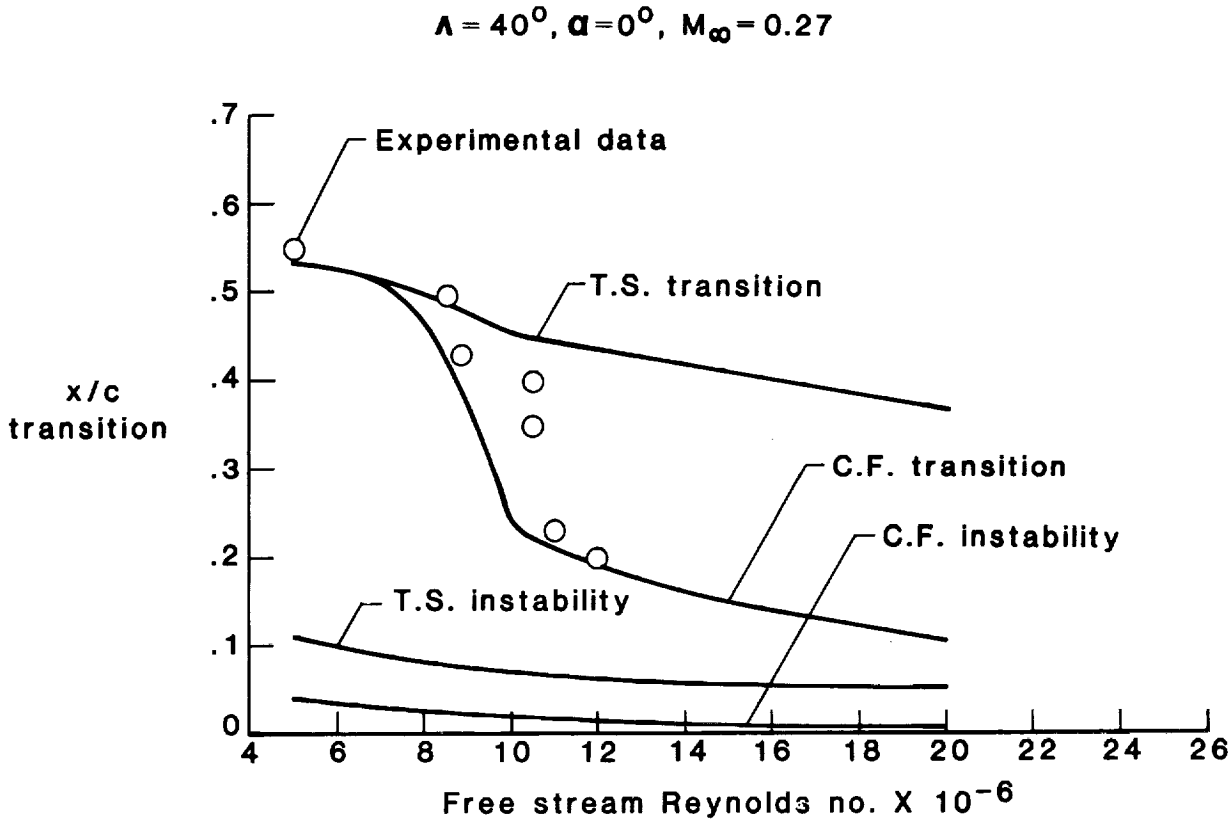

Figure 16

PLANFORM OF PHOENIX SAILPLANE AND AIRFOIL GEOMETRY

The planform of the Phoenix sailplane and the geometry of the airfoil at the test location on the wing are shown in figure 17. The pressure distributions and velocity profiles were measured by Raspet[9] at several chordwise locations at the test location for several values of lift coefficient. The maximum thickness-to-chord ratio for the test location airfoil is 0.15 and is located at x/c = 0.35. The maximum camber is located at x/c = 0.70. The aspect ratio of the wing is approximately 18.

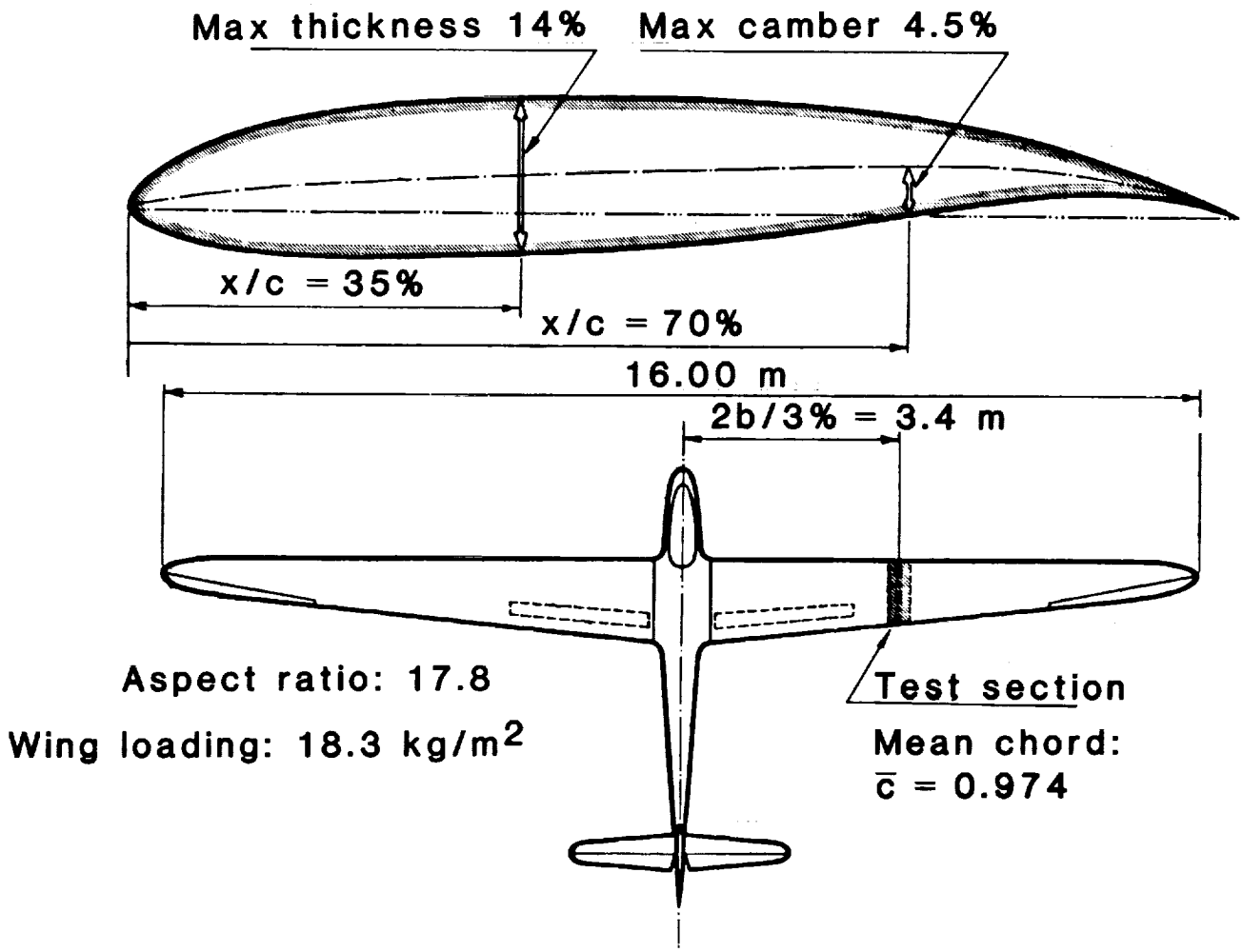

Figure 17

PRESSURE DISTRIBUTION CORRELATION ON PHOENIX WING
C_L = 0.76 AND R_N = 1.464 × 10^6

The comparison between the theoretical pressure distribution computed by the MCARF program and the experimental data of Raspet for the Phoenix wing at a lift coefficient of 0.76 and a chord Reynolds number of 1.464 million is shown in figure 18. The results plotted in this figure show that the computed pressure distribution agrees quite well with the measured experimental data. These computed and experimental pressure distributions were input as boundary conditions to the integral boundary-layer method used to compute the transition locations presented subsequently.

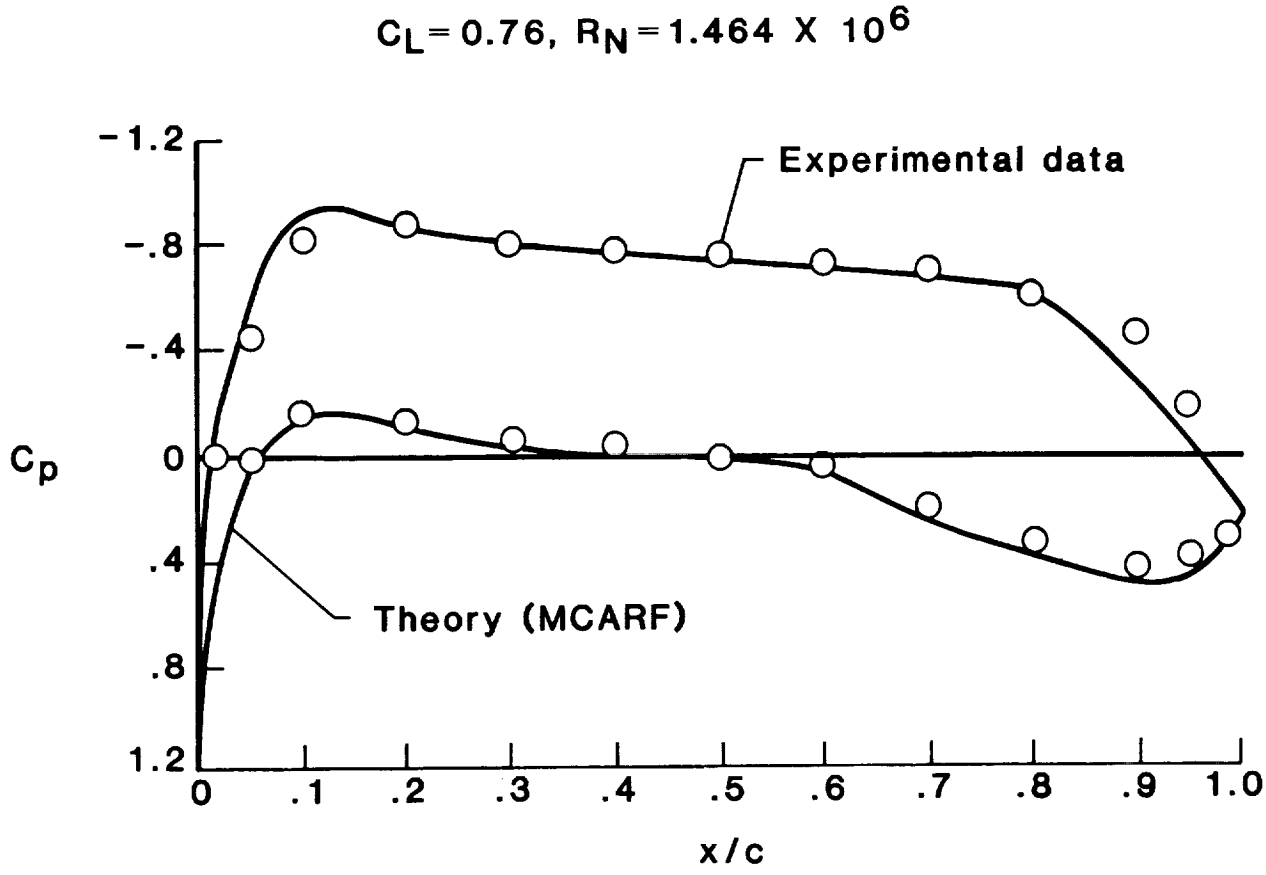

Figure 18

PRESSURE DISTRIBUTION CORRELATION ON PHOENIX WING
C_L = 1.14 AND R_N = 1.2 x 10^6

The comparison of pressure distribution computed by MCARF and the experimental data for Phoenix wing at lift coefficient of 1.14 and a chord Reynolds number of 1.2 million is presented in figure 19. The computed pressure distribution agrees fairly well with experimental data except near the trailing edge where turbulent boundary-layer separation is present.

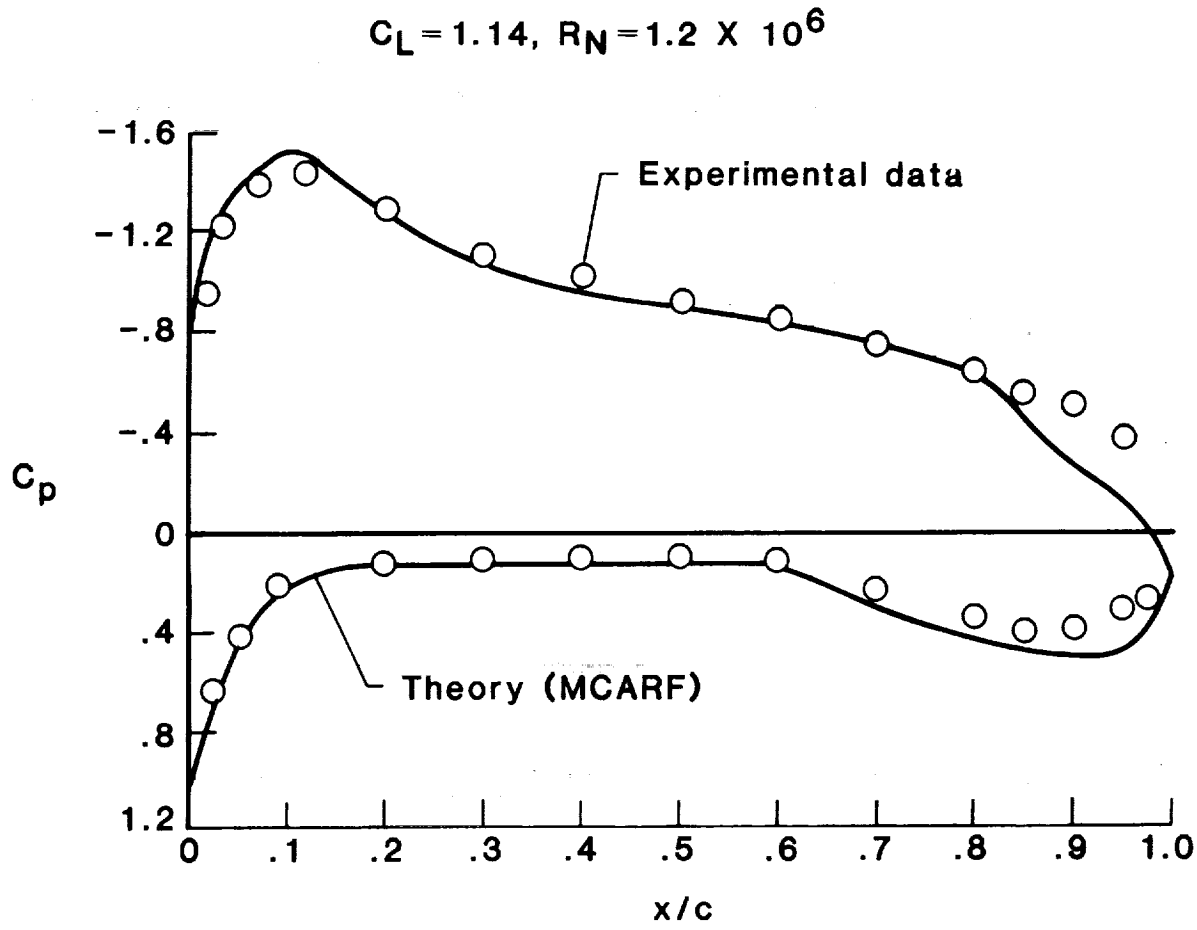

Figure 19

TRANSITION CORRELATION FOR PHOENIX SAILPLANE WING

The correlation for transition and turbulent separation locations on the test location airfoil of the Phoenix wing is presented in figure 20. The results are plotted as a function of lift coefficient. These results indicate that the chordwise location of turbulent separation is predicted fairly well. However, some discrepancy exists between the computed and experimental transition location for lift coefficients in the range of 0.6 to 1.1 when the theoretical pressure distributions were used as input boundary conditions. In order to examine the effect of using different boundary conditions, transition locations were also computed using experimental pressure distributions as input boundary conditions. As seen in figure 20, the difference in the theoretical transition locations using the two different boundary conditions is not significant. It should be emphasized that the author Raspet did not measure the location of transition directly but, instead, inferred the location from the measured velocity profiles; therefore, there may be some discrepancy in the actual measured transition locations.

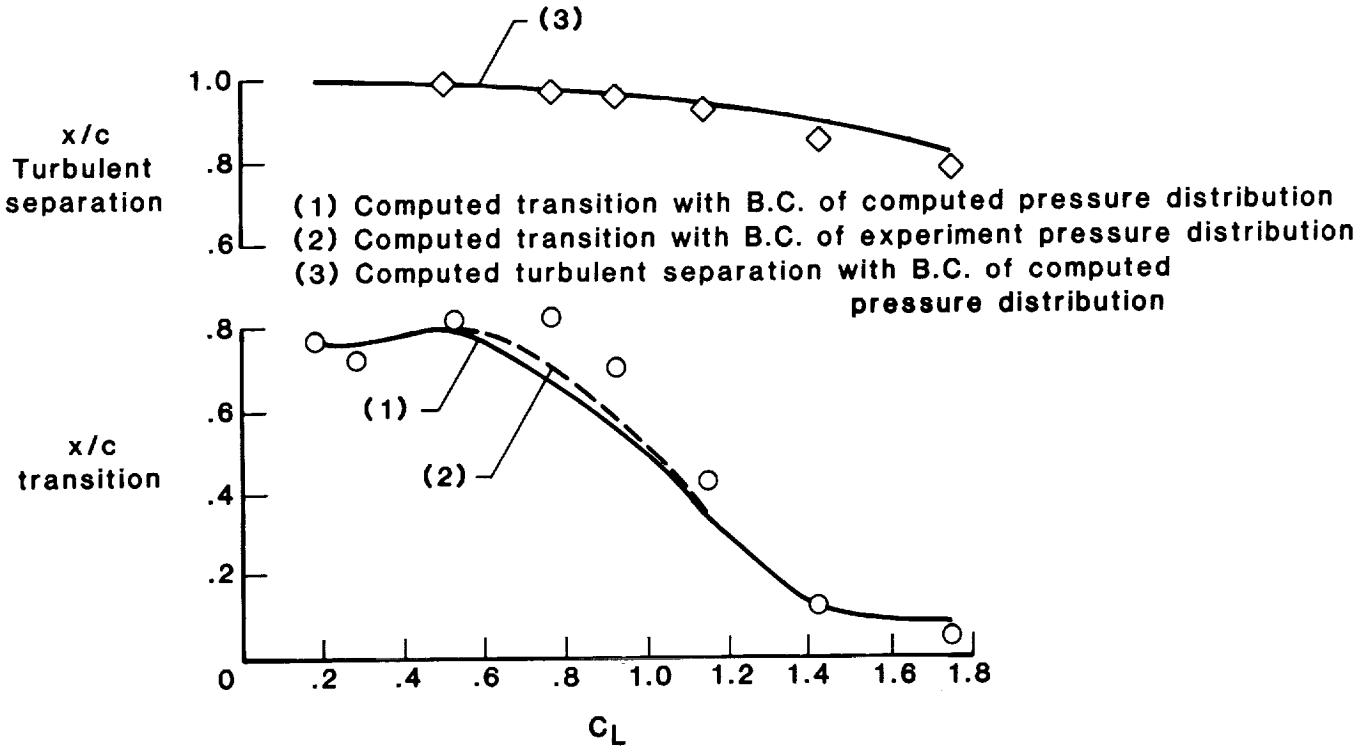

Figure 20

CORRELATION OF TRANSITION DATA FOR LFC WING WITH PARTIAL SUCTION
$\Lambda = 23°$ AND $M_\infty = 0.826$

The correlation of the transition locations for the NASA Langley LFC wing with partial suction on the upper surface are presented in figure 21. The chordwise location of suction was varied from an x/c of 0.0 to 0.5. The transition measurements were made at a free-stream Mach number of 0.826 and chord Reynolds numbers of 10 to 20 million. Theoretical computations were performed using boundary conditions of experimentally measured suction coefficients as input boundary conditions. The predicted transition locations are in good agreement with the measured transition locations. The results of the three correlation cases presented have demonstrated the validity of the new integral boundary-layer method.

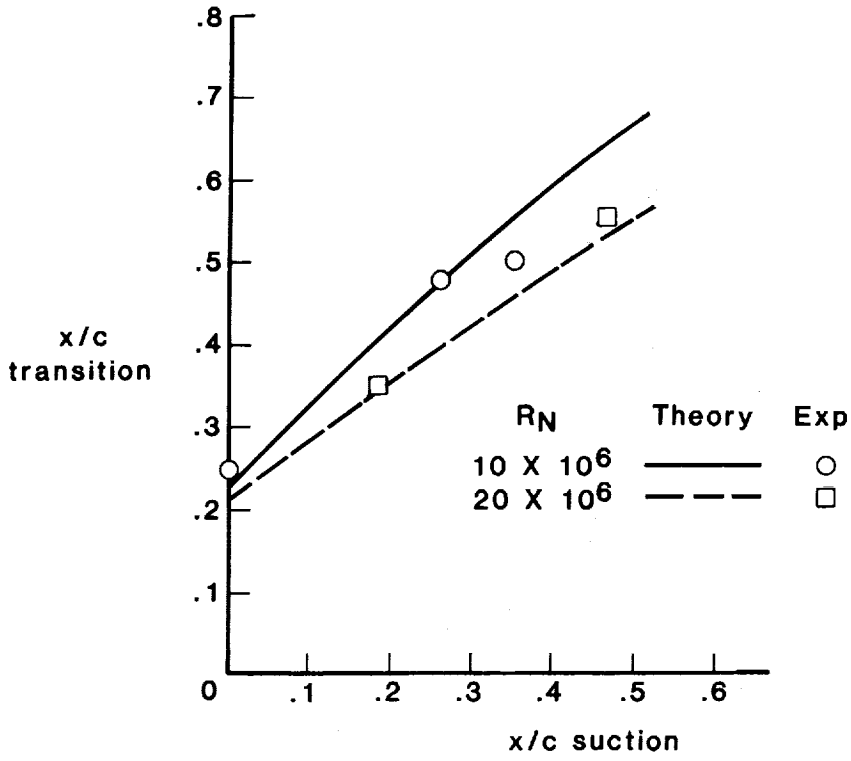

Figure 21

DESIGN CONSTRAINTS OF HYBRID LAMINAR-FLOW CONTROL WING

The design constraints and objectives for the Hybrid Laminar Flow Control (HLFC) wing to be tested in the Langley 8-Foot Transonic Pressure Tunnel are illustrated on figure 22. The design constraints and objectives that were laid out by Mr. P. J. Bobbitt, who also directed the HLFC design and optimization studies, are summarized as follows:

Design Constraints

(1) The geometry of the lower surface of the HLFC wing must be the same as that of the LFC wing.
(2) The geometry of the upper surface panel #1 of the HLFC wing must be identical to that on the present LFC wing and suction must be applied only through panel #1.
(3) The sonic bubble height for the HLFC wing must be no greater, and, if possible, smaller than that for the LFC wing.

Design Objectives

(1) The geometric shape of the upper surface panels #2 and #3 must be derived by the inverse perturbation method of characteristics so that laminar boundary-layer flow is maintained up to $x/c = 0.6$ on the upper surface of HLFC wing for $C_L = 0.45$ and $M_\infty = 0.82$.
(2) The computed turbulent separation location on the upper surface of the HLFC wing must be aft of $x/c = 0.95$.

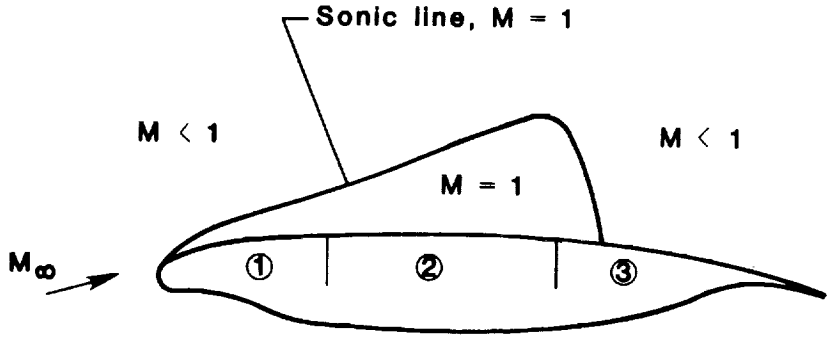

- Suction applied to panel 1
- Geometry of panels 2 and 3 altered for:
  - Sonic line height constraint
  - Laminar B.L. flow for $x/c \approx 0.6$
  - Turbulent separation aft of $x/c \approx 0.95$

Figure 22

COMPARISON BETWEEN THEORETICAL AND EXPERIMENTAL PRESSURE DISTRIBUTIONS FOR LFC AND HLFC WINGS

A comparison of pressure distributions between the design HLFC wing and the present LFC wing is presented in figure 23. The application of suction is limited to $0.025 \leq x/c \leq 0.26$ on the upper surface of the HLFC wing. The pressure distribution for the HLFC wing (shown by the dotted line) constitutes the boundary condition necessary to achieve the design constraints and objectives outlined on figure 22.

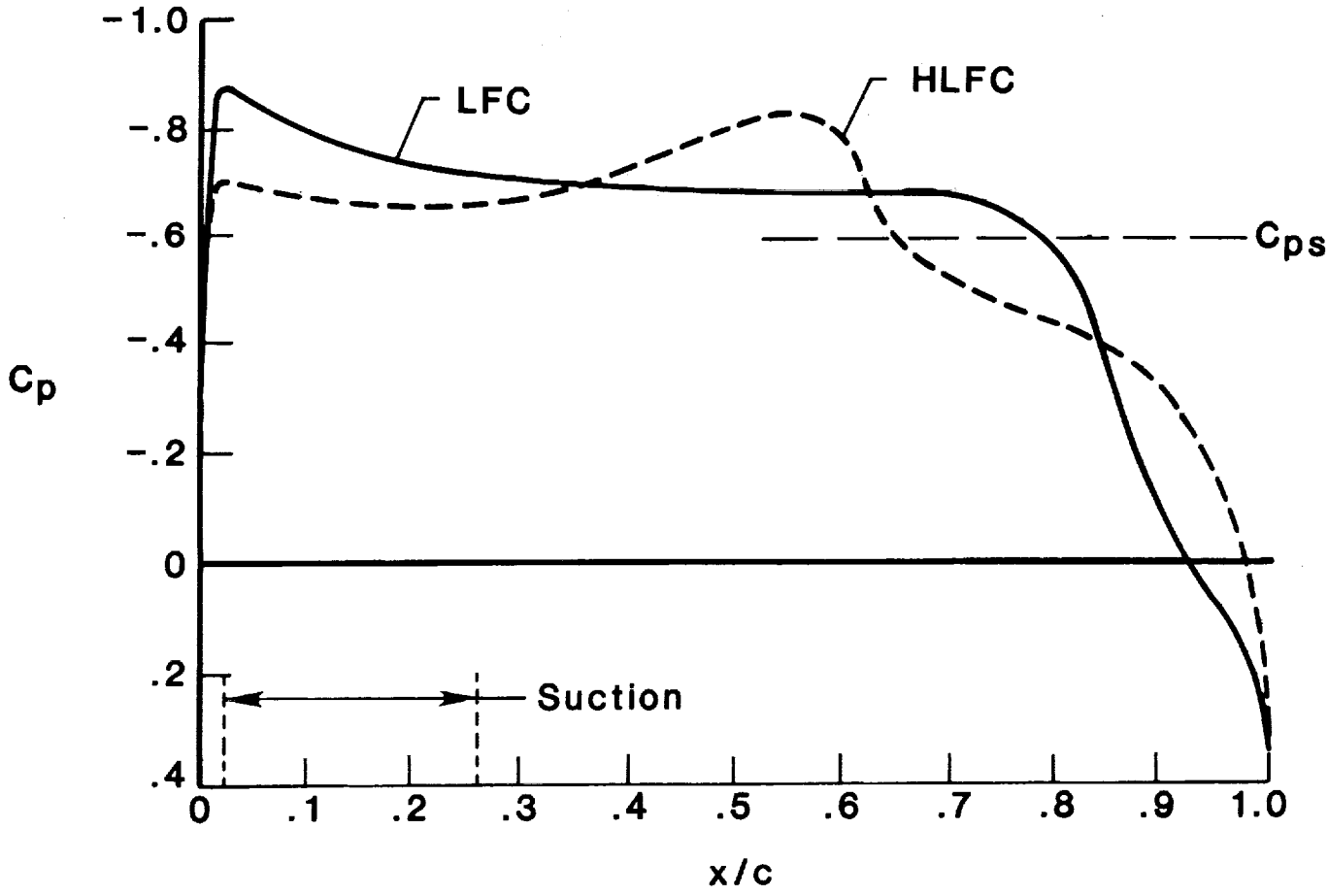

Figure 23

PREDICTED TRANSITION AND TURBULENT SEPARATION LOCATIONS FOR HLFC

The computational results for the predicted transition and turbulent boundary-layer separation locations on the upper surface of the HLFC wing are presented in figure 24. Predicted results are shown for transition due to Tollmien-Schlichting (T.S.) wave amplification, transition due to cross flow (C.F.), and instability due to T.S. and C.F. The chordwise location of computed turbulent separation is also presented. These results are plotted as a function of free-stream Reynolds number and for a wing $C_L = 0.44$ and free-stream $M_\infty = 0.811$.

As shown in figure 24, transition due to T.S. with short bubble reattachment occurs at $x/c = 0.58$ for the range of Reynolds numbers shown. However, transition due to C.F. takes over at a Reynolds number of 15 million. It is assumed with the present theory that the transition occurs on the wing due to whichever phenomena appears first. Thus, cross flow essentially determines the transition location at the higher Reynolds number. In addition, there is a danger of leading-edge contamination due to C.F. instability at Reynolds numbers larger than approximately 20 million. The computed turbulent separation location is downstream of $x/c = 0.95$ for the entire range of Reynolds numbers.

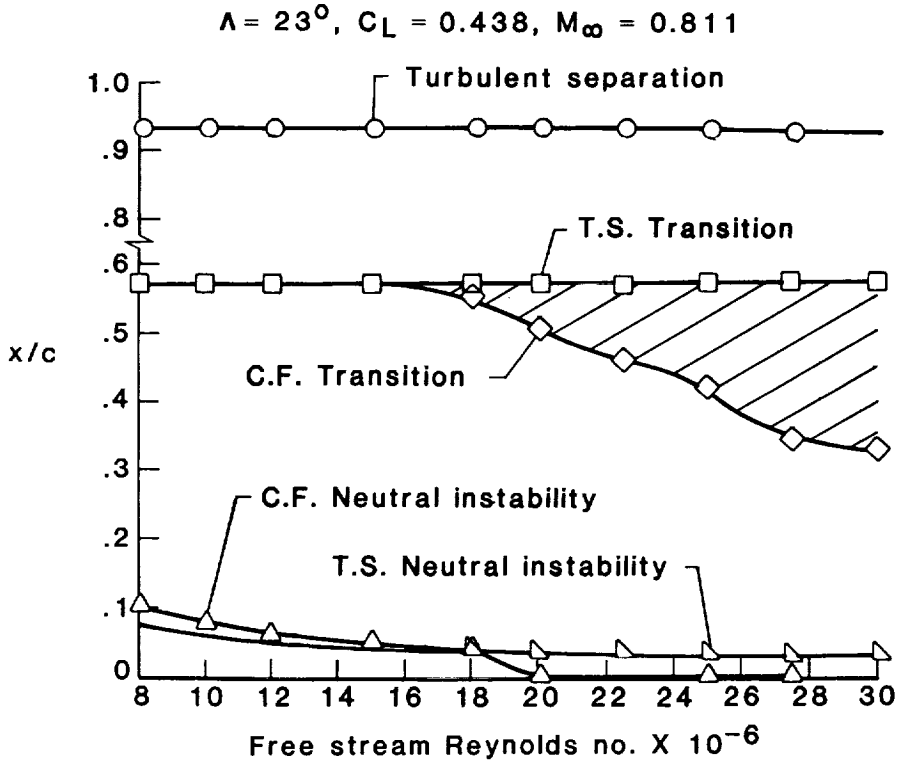

Figure 24

CONCLUSIONS AND RECOMMENDATIONS

The results of the design studies of the HLFC wing using the integral boundary-layer methods of Goradia lead to the following conclusions and recommendations:

(1) The perturbation method of characteristics was found to be extremely useful for determining the geometric changes needed in the baseline LFC airfoil shape to obtain the desired HLFC pressure distribution.

(2) The compressible laminar boundary-layer method with suction was found to be quite accurate in predicting the extent of laminar flow for swept wings in the presence of suction. Also with this method the suction requirements can be determined for different local velocity profiles such as those for Blasius, separating laminar, or asymptotic suction velocity distributions.

(3) The turbulent boundary-layer separation method includes terms to account for the rapid increase in the turbulent fluctuations in the flow near separation; these terms greatly improved the accuracy of the prediction of the location of turbulent separation.

(4) The integral boundary-layer methods execute very rapidly on the computer making it possible to analyze several hundred configurations in a relatively short period of time.

(5) The results of the correlative studies generally showed excellent agreement between the theoretical predictions and the experimental data. The results also showed that, for values of Reynolds number and wing sweep of practical interest for commercial and fighter aircraft, cross-flow instabilities were predominant in triggering transition.

(6) The analysis of the final HLFC design showed that less than one count of suction drag coefficient was required in conjunction with the appropriate pressure distribution to achieve laminar flow on the upper surface of the wing to the 60-percent chord location. This one count of suction drag results in a corresponding 30 to 40 count reduction in the wake drag coefficient which suggests that HLFC is a very lucrative and promising concept for viscous drag reduction at both transonic and supersonic speeds.

(7) In order to prevent laminar transition due to cross flow at large values of sweep and Reynolds number, it is recommended that both the chordwise and the spanwise pressure gradients be tailored to minimize the growth of the boundary-layer disturbances. With the use of a modified strip theory, arbitrary spanwise pressure gradients can be accounted for when using the present integral boundary-layer methods.

The present integral boundary-layer methods have been extended to compute both laminar and turbulent boundary-layer flow and to predict transition locations at supersonic Mach numbers. The effects of variations in temperature profile and physical flow properties across the boundary layer, suction, wing sweep, wing taper, and wing twist are also accounted for in these methods. These methods are not limited to wings alone, but can also be used for the analysis of fighter aircraft fuselage with suction at supersonic flight conditions. Correlation studies are currently under way to determine the validity of these extended integral boundary-layer methods.

REFERENCES

1. Harvey, William D.; Harris, Charles D.; Brooks, Cyler W. Jr.; Clukey Patricia G.; Bobbitt, Percy J.; and Stack, John P.: Design and Experimental Evaluation of a Swept Supercritical LFC Airfoil. NASA CP-2398, Vol. I, Langley Symposium on Aerodynamics, April 23-25, 1985.

2. Meyer, W. D.; and Jennett, L. A.: In Flight Surface Oil Flow Photographs with Comparison to Pressure Distributions and Boundary-Layer Data. NASA TP 2393, April 1985.

3. Goradia, S. H.: The Method of Characteristics Perturbation Technique as Applied to Airfoil Design. Lockheed-Georgia Company Advanced Design Aerodynamics Memorandum 13-68, March 1968.

4. Bauer, F; Garabedian, P.; and Korn, D.: A Theory of Supercritical Wing Sections, with Computer Programs and Examples. Volume 66 of Lecture Notes in Economics and Mathematical Systems, Springer-Verlag, 1972.

5. Stevens, W. A.; Goradia, S. H.; and Braden, J. A.: Mathematical Model for Two-Dimensional, Multi-Component Airfoils in Viscous Flow. NASA CR-1843, 1971.

6. Goradia, S. H.; and Lyman, V. L.: Laminar Stall Prediction and Estimation of CL_{max}. Journal of Aircraft, Vol. 11, No. 9, pp 528-536, Sept. 1974.

7. Goradia, S. H.; and Morgan, H. L. Jr.: A New, Improved Method for Separating Turbulent Boundary Layer for Aerodynamic Performance Predictions of Trailing Edge Stall Airfoils. AIAA Paper 86-1832-CP, presented at AIAA 4th Applied Aerodynamics Conference, San Diego, California, June 9-11, 1986.

8. Boltz, F. W.; Kenyon, G. C.; and Allen, C. Q.: Effects of Sweep Angle on the Boundary-Layer Stability Characteristics of an Untapered Wing at Low Speeds. NASA TN D-338, 1960.

9. Raspet, A.; Gyorgy-Falvy, D.; and Cornish, J.: Boundary Layer Studies on Phoenix Sailplane. Presented at the VIII Congress of O.S.T.I.V., Koln, Germany, June 1960.